

STRUCTURAL AND TEMPERATURE DEPENDENT DIELECTRIC PROPERTIES OF TIN SUBSTITUTED COBALT FERRITES ($\text{Sn}_x\text{Co}_{1-x}\text{Fe}_2\text{O}_4$)

S. ANJUM*, A. MASUD

Department of Physics, Lahore College for Women University, Lahore, Pakistan

A string of tin doped cobalt ferrites $\text{Sn}_x\text{Co}_{1-x}\text{Fe}_2\text{O}_4$ where ($x=0, 0.2, 0.4, 0.6, 0.8, 1$) samples have been prepared using powder metallurgy route, annealed at 1200°C . The structural analysis is accomplished using X-ray diffractometer. This analysis confirms that all the prepared samples have inverse cubic spinel structure. It is also revealed that the crystallite size and lattice parameter increase with the increasing concentration of tin (Sn^{2+}) ions. This is due to the larger ionic radii of tin. The 3D visualization of XRD data is simulated using diamond software. The dielectric properties of the prepared tin ferrites have been determined using inductor capacitor resistor (LCR) meter. An extensive analysis of frequency, concentration and temperature dependent dielectric properties of the synthesized samples are described in this paper. It is concluded that the dielectric constant and dielectric loss have been decreased and conductivity is increased as the frequency increases. The observed value of high-dielectric constant and dielectric tangent loss response at low frequencies has been attributed due to the presence of grain boundaries in these ferrites. Temperature acts as a significant factor in the enhancement of the dielectric constant, dielectric loss and a.c. conductivity owing to the mobility of ions which increases as the temperature increase.

(Received April 4 2018; Accepted November 5, 2018)

Keywords: Crystallite size, Annealing temperature, Dielectric constant, A. C conductivity, Hopping length

1. Introduction

Spinel ferrites fall in the category of semiconductor ceramics and have high dielectric constant that are of considerable interest due to their potential applications in the future technology. Cobalt ferrite is used in magnetic, magneto-optical recording, electromagnetic, and spintronics devices [1]. The electrical properties strongly depend on the composition, annealing conditions, grain sizes, and dopant materials [2]. Dielectric properties of cobalt ferrite have been studied with various dopant materials and concentrations [3-4]. In most of these studies, a decrease of dielectric constant and conductivity of the materials with dopant concentration has been reported. Contrary to the previous analyses, we report an increasing behavior of conductivity and dielectric constant with doping of tin in cobalt ferrites. The materials with high-dielectric constants have become immense interest for the miniaturized memory devices that are based on the capacitive components or energy storage principles [5-6]. The high values of dielectric constant at various frequencies of $\text{La}_{1.5}\text{Sr}_{0.5}\text{NiO}_4$ have been investigated on the basis of charge ordering (CO) [7].

Several reports are available on the electrical conductivity and dielectric properties of bulk cobalt ferrite [8, 9]. Jonker [10] has studied the electrical properties of a series of bulk $\text{Co}_{3-x}\text{Fe}_x\text{O}_4$ ferrites and observed two region of conductivity. The hole hopping between Co^{2+} and Co^{3+} ions contributes to the low-conductivity regions and the electron hopping between Fe^{2+} and Fe^{3+} ions is found to be responsible for the high conductivity region. Na et al. [11] have reported the mechanism for electrical conduction for bulk CoFe_2O_4 under various heat treatment conditions.

*Corresponding author: safia_anjum@hotmail.com

They have also observed a decrease in the electrical resistivity with quenching temperature, which is mainly because of the decrease in grain boundary resistance in Fe-excess cobalt ferrites.

In current research work a series of tin doped cobalt ferrite $\text{Sn}_x\text{Co}_{1-x}\text{Fe}_2\text{O}_4$ where ($x=0, 0.2, 0.4, 0.6, 0.8, 1$) has been synthesized using powder metallurgy route. The prepared samples have been characterized structurally and also show their structure in 3D visualization. The comprehensive study of dielectric properties has been carried out using LCR meter. The frequency, temperature and concentration dependent dielectric properties are studied in detail. It is report that the grain boundary is responsible for the high dielectric constant at lower frequencies. Their dielectric constant and capacitance at low frequency are studied in detail. The conductivity and dielectric constant values are found to enhance with doping of tin in cobalt ferrites.

2. Experimental setup

The schematic diagram of experimental setup is shown in figure 1. The starting materials Fe_2O_3 , SnO and CoO powders are 99.99% pure. The specific quantity of the materials according to the stoichiometry calculation is grinded in a ball milling machine, until homogeneous mixture is obtained. The mixture is then heat treated at 1200 °C for 2h in Lindberg USA model blue M. BF51524C furnace and cooled down inside the furnace. The calcined powders are then re-grinded to form homogenous powder using A-gate motor-pastel.

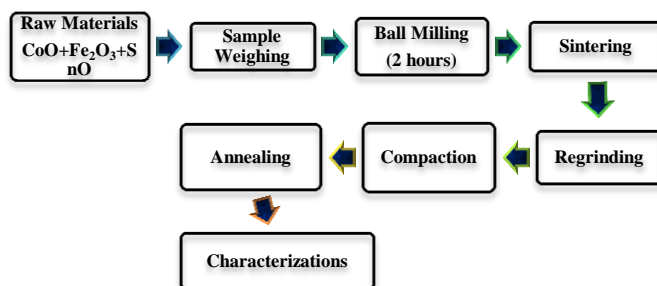


Fig. 1. Block diagram of sample preparation

2.1 Characterization techniques

The prepared samples of tin substituted cobalt ferrite have been characterized using X-ray diffractometer, diamond software and LCR meter. The structural characterization of samples is carried out by X-ray diffractometer (D-8 discover, Bruker, Germany, source scintillation $\text{CuK}\alpha$ radiation (1.5406Å) detector; eudetube current = 40mA, tube voltage = 40 kV, scan speed = 3°/min increment = 0.05°). The temperature dependent impedance spectroscopy was performed using LCR meter Quad Tech 1920 in the frequency range of 1 kHz to 1 MHz.

3. Results and discussions

3.1 XRD analysis

The XRD pattern of $\text{Sn}_x\text{Co}_{1-x}\text{Fe}_2\text{O}_4$ is shown in figure 2. The peaks of XRD micrographs show that all samples of the prepared samples of cobalt ferrites have cubic inverse spinel phase structure. The diffraction peaks (220), (311), (400), (422), (511) and (440) are confirmed by XRD micrographs that are accurately coordinated by JCPDC card No. 22-108 [12]. It is observed that the sample of prepared tin doped cobalt ferrites have no secondary phase and belongs to Fd-3m space group.

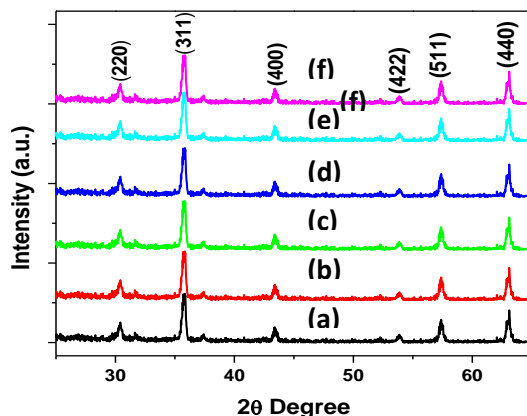


Fig. 2. XRD micrographs of $\text{Sn}_x\text{Co}_{1-x}\text{Fe}_2\text{O}_4$ at (a) $x=0.0$, (b) $x=0.2$, (c) $x=0.4$, (d) $x=0.6$, (e) $x=0.8$, (f) $x=1.0$

The Bragg's law statement is being used to calculate the d-spacing which is given by [13]:

$$n\lambda = 2d\sin\theta \quad (1)$$

The lattice parameter has been evaluated by the formula [14]:

$$a = d \cdot (h^2 + k^2 + l^2)^{1/2} \quad (2)$$

The crystallite size is measured using Scherer's formula expressed as [15]:

$$D_p = K\lambda/\beta\cos\theta \quad (3)$$

where, K is the shaping factor having value of 0.94, D_p is the crystallite size, λ is the wavelength of Cu K_α (1.54 nm), β is the full wave half maximum. The dislocation line density is evaluated as [16]:

$$\sigma = 1/D_p^2 \quad (4)$$

X-ray density is evaluated by following equation [17]:

$$d_x = 8M/\text{Na}^3 \quad (5)$$

The highest peak of (311) from the XRD graph has been used to study the XRD parameters such as lattice parameter, crystallite size, dislocation line density and x-ray density that are listed in Table 1.

Table 1. XRD parameters for tin substituted cobalt ferrites

Composition	Molecular Weight(g)	FWHM (A°)	d-spacing (A°)	Lattice parameter (A°)	Crystallite size (nm)	x-ray density (g/nm^3)
$\text{Sn}_0\text{Co}_1\text{Fe}_2\text{O}_4$	47	0.3542	2.50403	8.304	24.59	1.09
$\text{Sn}_{0.2}\text{Co}_{0.8}\text{Fe}_2\text{O}_4$	51	0.1574	2.50924	8.322	24.61	1.17
$\text{Sn}_{0.4}\text{Co}_{0.6}\text{Fe}_2\text{O}_4$	56	0.3542	2.51213	8.331	24.62	1.28
$\text{Sn}_{0.6}\text{Co}_{0.4}\text{Fe}_2\text{O}_4$	59	0.2755	2.51948	8.356	31.65	1.34
$\text{Sn}_{0.8}\text{Co}_{0.2}\text{Fe}_2\text{O}_4$	64	0.3542	2.52098	8.360	50.39	1.45
$\text{Sn}_1\text{Co}_0\text{Fe}_2\text{O}_4$	69	0.1574	2.5209	8.361	55.42	1.51

The graph of crystallite size and lattice parameter as a function of tin concentration is shown in Fig. 3. It is revealed that the lattice parameter and crystallite size increases with the increasing Sn^{+2} concentrations. This transpires due to the relative size of the ionic radii of the dopant. The ionic radius of Sn^{+2} (1.12 \AA) which is larger than the ionic radii of Co^{+2} (0.78 \AA) therefore replacement of cobalt with tin causes the expansion in unit cell, hence the lattice parameter increases [18].

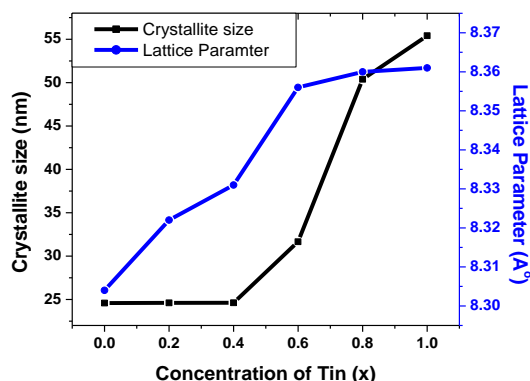


Fig. 3. Lattice parameter and crystallite size as a function of Sn^{2+} contents

The x-ray density increases with the increasing amount of Sn^{+2} ions as shown in Fig. 4 which depends on the atomic weight of cobalt and tin atoms. As the atomic weight of tin 118.71 amu which is greater as compared to the atomic weight of cobalt 58.934 amu , thus smaller weight ion are replaced by large weight ions causing a linearly increase in the x-ray density.

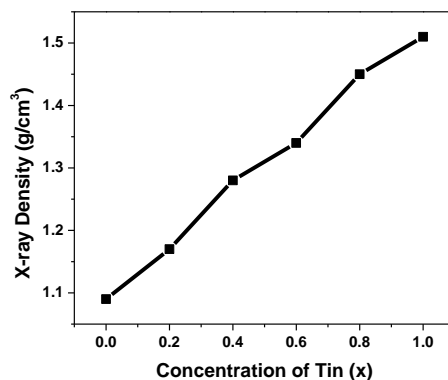


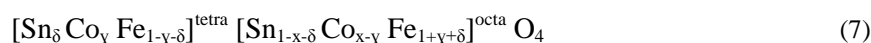
Fig. 4. X-ray density as function of Sn^{2+} concentration

3.1.1 Estimation of cationic distribution

It is evident from the XRD analysis that cobalt ferrites have inverse cubic spinel structure. This type of structure mainly comprises of two sites which are named as A (tetrahedral) site and B (octahedral) site. The iron cations are distributed uniformly between the two sites whereas cobalt ions prefer to occupy B sites. Tin ions usually occupies the octahedral site. The cation distribution among the sites A and B site is expressed as [19]:



The former fragment of the equation articulates that the cations at A site, whereas the latter fragment shows the cations at B- site. γ is considered as a constant known as degree of inversion between the two sites. The cation distribution for the sample to be investigated i.e. $\text{Sn}_x\text{Co}_{x-1}\text{Fe}_2\text{O}_4$ ($x=0, 0.2, 0.4, 0.6, 0.8$ and 1.0) is as follows [20]:



$$r_{\text{tetra}} = \delta r_{\text{Sn}} + \gamma r_{\text{Co}} + (1+\gamma-\delta)r_{\text{Fe}} \quad (8)$$

$$r_{\text{octa}} = 1/2[(1-x-\delta)r_{\text{Sn}} + (x-\gamma)r_{\text{Co}} + (1+\gamma+\delta)r_{\text{Fe}}] \quad (9)$$

The estimated cation distribution is listed in table 2. Besides this, the mean ionic radii of cations existing at both tetrahedral and octahedral sites are given by the equations, respectively [21].

$$r_{\text{tetra}} = a\sqrt{3} (u-0.25) - R_o \quad (10)$$

$$r_{\text{octa}} = a (5/8 - u) - R_o \quad (11)$$

$R_o = 1.26\text{\AA}$, represents the oxygen radius, u is the oxygen parameter and γ can be calculated using the above equations simultaneously.

Table 2. Estimated cation distribution for $\text{Sn}_x\text{Co}_{1-x}\text{Fe}_2\text{O}_4$

Composition of Sn (x)	Tetrahedral site (A)	Octahedral site (B)
$\text{Sn}_0\text{Co}_1\text{Fe}_2\text{O}_4$	Co(0.02)Fe(0.98)	Co(0.98)Fe(1.2)
$\text{Sn}_{0.2}\text{Co}_{0.8}\text{Fe}_2\text{O}_4$	Sn(0.1)Co(0.3)Fe(0.6)	Sn(0.1)Co(0.5)Fe(1.4)
$\text{Sn}_{0.4}\text{Co}_{0.6}\text{Fe}_2\text{O}_4$	Sn(0.1)Co(0.2)Fe(0.7)	Sn(0.3)Co(0.4)Fe(1.3)
$\text{Sn}_{0.6}\text{Co}_{0.4}\text{Fe}_2\text{O}_4$	Sn(0.1)Co(0.1)Fe(0.8)	Sn(0.5)Co(0.3)Fe(0.2)
$\text{Sn}_{0.8}\text{Co}_{0.2}\text{Fe}_2\text{O}_4$	Sn(0.1)Co(0.1)Fe(0.8)	Sn(0.7)Co(0.1)Fe(1.2)
$\text{Sn}_1\text{Co}_0\text{Fe}_2\text{O}_4$	Sn(0.1)Fe(0.9)	Sn(0.9) Fe(1.1)

Hopping length is the distance between magnetic ions at A and B site, which is determined by the relation [22]:

$$d_A = 0.25a\sqrt{3} \quad (12)$$

$$d_B = 0.25a\sqrt{2} \quad (13)$$

a is the lattice parameter. The hopping length at tetrahedral (d_A) and octahedral site (d_B) of all the samples are tabulated in Table 3.

Table 3. Hopping length at tetrahedral and octahedral site

Composition of Sn (x)	A site(d_A) \AA	B site(d_B) \AA
$\text{Sn}_0\text{Co}_1\text{Fe}_2\text{O}_4$	3.596	2.936
$\text{Sn}_{0.2}\text{Co}_{0.8}\text{Fe}_2\text{O}_4$	3.603	2.942
$\text{Sn}_{0.4}\text{Co}_{0.6}\text{Fe}_2\text{O}_4$	3.607	2.945
$\text{Sn}_{0.6}\text{Co}_{0.4}\text{Fe}_2\text{O}_4$	3.618	2.956
$\text{Sn}_{0.8}\text{Co}_{0.2}\text{Fe}_2\text{O}_4$	3.620	2.958
$\text{Sn}_1\text{Co}_0\text{Fe}_2\text{O}_4$	3.619	2.960

The graph of d_A and d_B as a function of Sn concentration is shown in Fig. 5, which shows that hopping length increases with the increasing substitution of tin because the ionic radii of Sn^{+2} (1.12\AA) is greater than the ionic radii of Co^{+2} (0.78\AA) [23].

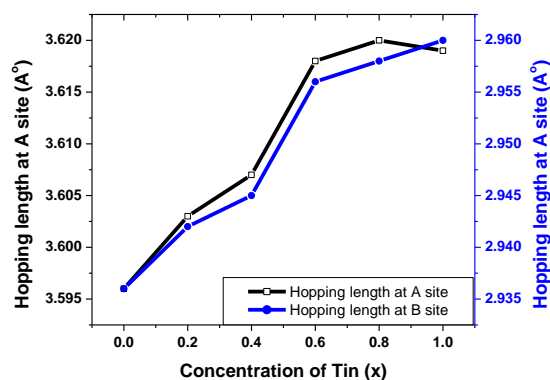


Fig. 5. Hopping length as a function of tin concentration

3.2 3D-visualisation

The 3-D visual of $\text{Sn}_x\text{Co}_{1-x}\text{Fe}_2\text{O}_4$ ferrites at various angles can be viewed by diamond software, as shown in Fig. 6. Diamond is an excellent software for molecular and crystal structure visualization and simulation. The XRD verifies that the peak intensities are well matched with the cubic inverse spinel structure of cobalt ferrites having space group $\text{Fd-}3\text{m}(227)$. The wyckoff positions and x, y, z coordinates of $\text{Sn}_x\text{Co}_{1-x}\text{Fe}_2\text{O}_4$ are listed in the Table 4.

Table 4. Atomic coordinates of $\text{Sn}_x\text{Co}_{1-x}\text{Fe}_2\text{O}_4$

Atoms	Oxidation number	Wyckoff site	X	Y	Z
O	-2	32e	0.25493	0.25493	0.25493
Sn	+2	8a	0	0	0
Co	+2	8b	$\frac{1}{2}$	$\frac{1}{2}$	$\frac{1}{2}$
Fe	+3	8b	$\frac{1}{2}$	$\frac{1}{2}$	$\frac{1}{2}$
Sn	+2	8b	$\frac{1}{2}$	$\frac{1}{2}$	$\frac{1}{2}$
Co	+2	16c	$\frac{1}{8}$	$\frac{1}{8}$	$\frac{1}{8}$
Fe	+3	16c	$\frac{1}{8}$	$\frac{1}{8}$	$\frac{1}{8}$
Sn	+2	16c	$\frac{1}{8}$	$\frac{1}{8}$	$\frac{1}{8}$
Co	+2	16d	$\frac{5}{8}$	$\frac{5}{8}$	$\frac{5}{8}$
Sn	+2	16d	$\frac{5}{8}$	$\frac{5}{8}$	$\frac{5}{8}$
Co	+2	16d	$\frac{5}{8}$	$\frac{5}{8}$	$\frac{5}{8}$

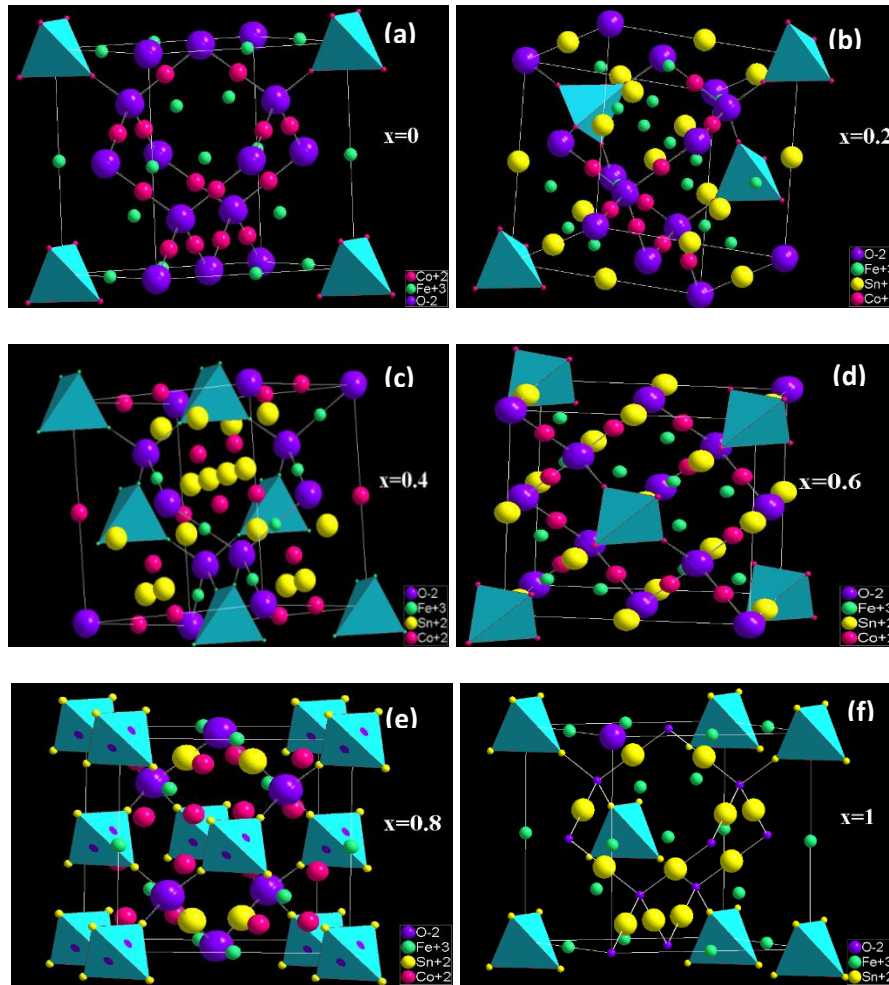


Fig. 6. 3D visualization of $\text{Sn}_x\text{Co}_{1-x}\text{Fe}_2\text{O}_4$ at (a) $x=0.0$, (b) $x=0.2$, (c) $x=0.4$, (d) $x=0.6$, (e) $x=0.8$, (f) $x=1.0$

3.3 Dielectric properties

The dielectric properties such as dielectric constant (ϵ'), tangent loss (ϵ'') and ac conductivity (σ_{ac}) of $\text{Sn}_x\text{Co}_{1-x}\text{Fe}_2\text{O}_4$ with ($x=0, 0.2, 0.4, 0.6, 0.8, 1$) have been evaluated using LCR meter. The dielectric parameters have been tailored at different temperatures .i.e. from 25°C to 200°C with the interval of 5°C at frequency range of 1kHz, 10kHz, 100kHz, 500kHz and 1MHz.

For dielectric measurements, the prepared ferrites were pressed to form circular pellets with thickness and diameter of 2 and 10 mm, respectively. The contacts were made on the opposite faces of the pellet using silver paint and copper wires of 12 inches length.

The values of dielectric constant (ϵ') are determined by the formula [24]:

$$\epsilon' = C_p d / \epsilon_o A \quad (14)$$

where, C is the capacitance of the pellet, ϵ_o is the permittivity of free space, A is cross sectional area and d is the thickness of pellet.

The dielectric loss (ϵ'') can be calculated using the relation [25]:

$$\epsilon'' = \epsilon' \tan \delta \quad (15)$$

$\tan \delta$ is tangent loss, which is ratio between total current and charging current.

The conductivity is calculated by [26]:

$$\sigma_{ac} = 2\pi f \epsilon_0 \epsilon' \tan\delta \quad (16)$$

where, f is the frequency, ϵ_0 permittivity of space, ϵ' is dielectric constant and $\tan\delta$ is tangent loss.

3.3.1 Dielectric constant (ϵ'), dielectric loss (ϵ'') and ac conductivity (σ_{ac}) as a function of Sn^{2+} concentration

The observed trend of the dielectric properties of cobalt ferrites is mainly influenced by cation distribution, sintering temperature, grain size, method of preparation, oxygen parameters, the ratio of Fe^{3+} ions and oxygen anion vacancies in the lattices [27]. The dependency of dielectric constant (ϵ'), dielectric loss (ϵ'') and ac conductivity (σ_{ac}) as a function of tin concentration is shown in Fig. 7(a), (b), (c), (d), (e), Fig. 8 (a), (b), (c), (d), (e), Fig. 9 (a), (b), (c), (d), (e) respectively.

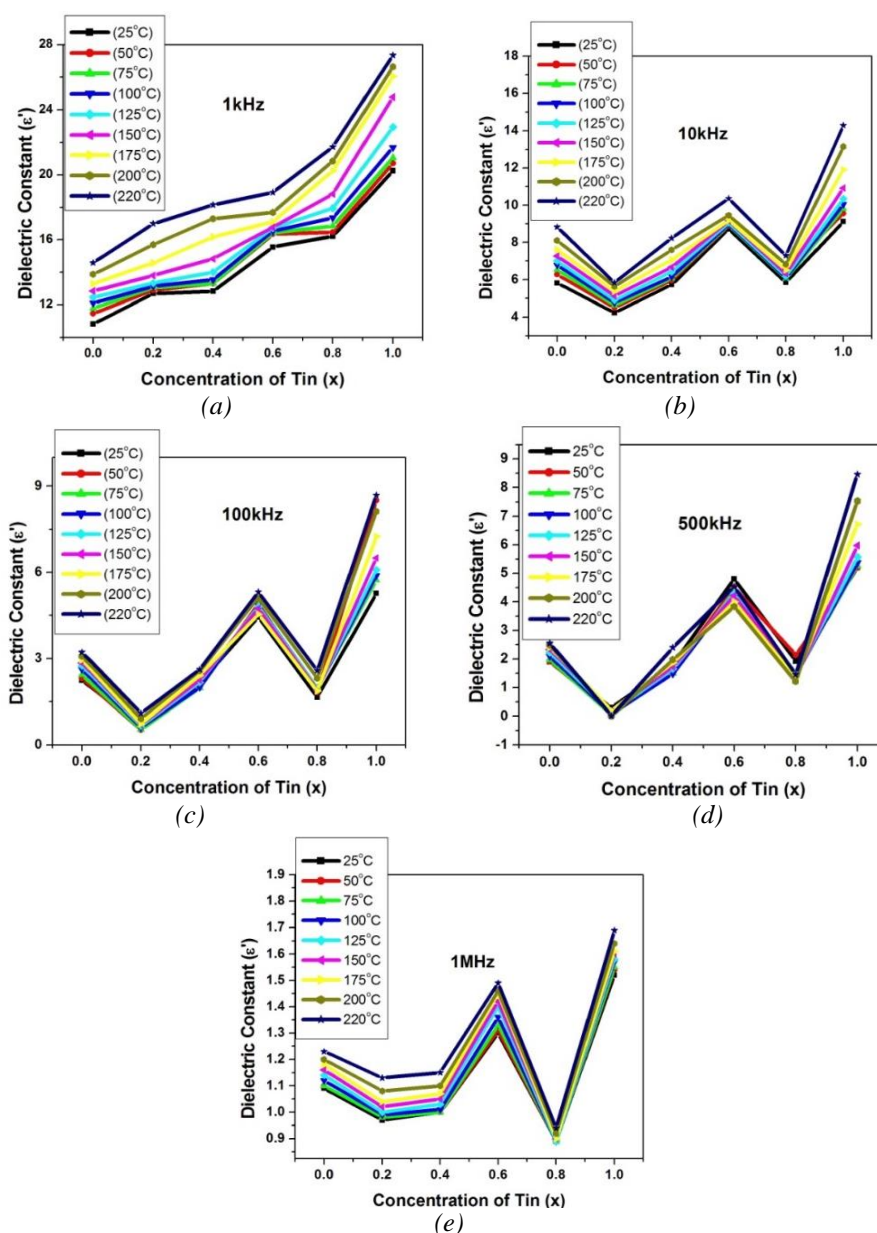


Fig. 7. Dielectric constant (ϵ') as a function of concentration of $\text{Sn}_x\text{Co}_{1-x}\text{Fe}_2\text{O}_4$ at frequency (a) 1kHz (b) 10kHz, (c) 100kHz, (d) 500kHz, (e) 1 MHz

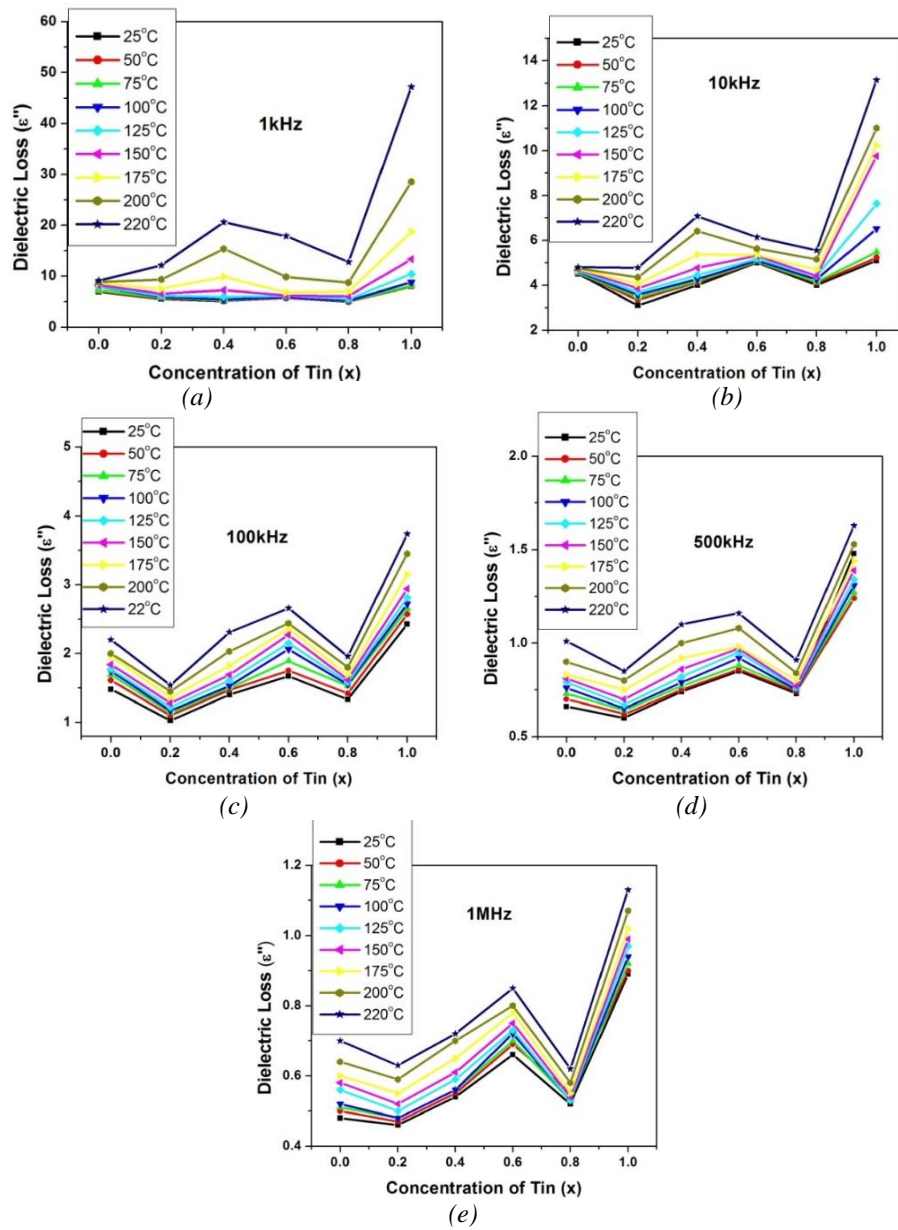


Fig. 8. Dielectric loss (ϵ'') as a function of concentration of $\text{Sn}_x\text{Co}_{1-x}\text{Fe}_2\text{O}_4$ at frequency (a) 1kHz (b) 10kHz, (c) 100kHz, (d) 500kHz, (e) 1 MHz

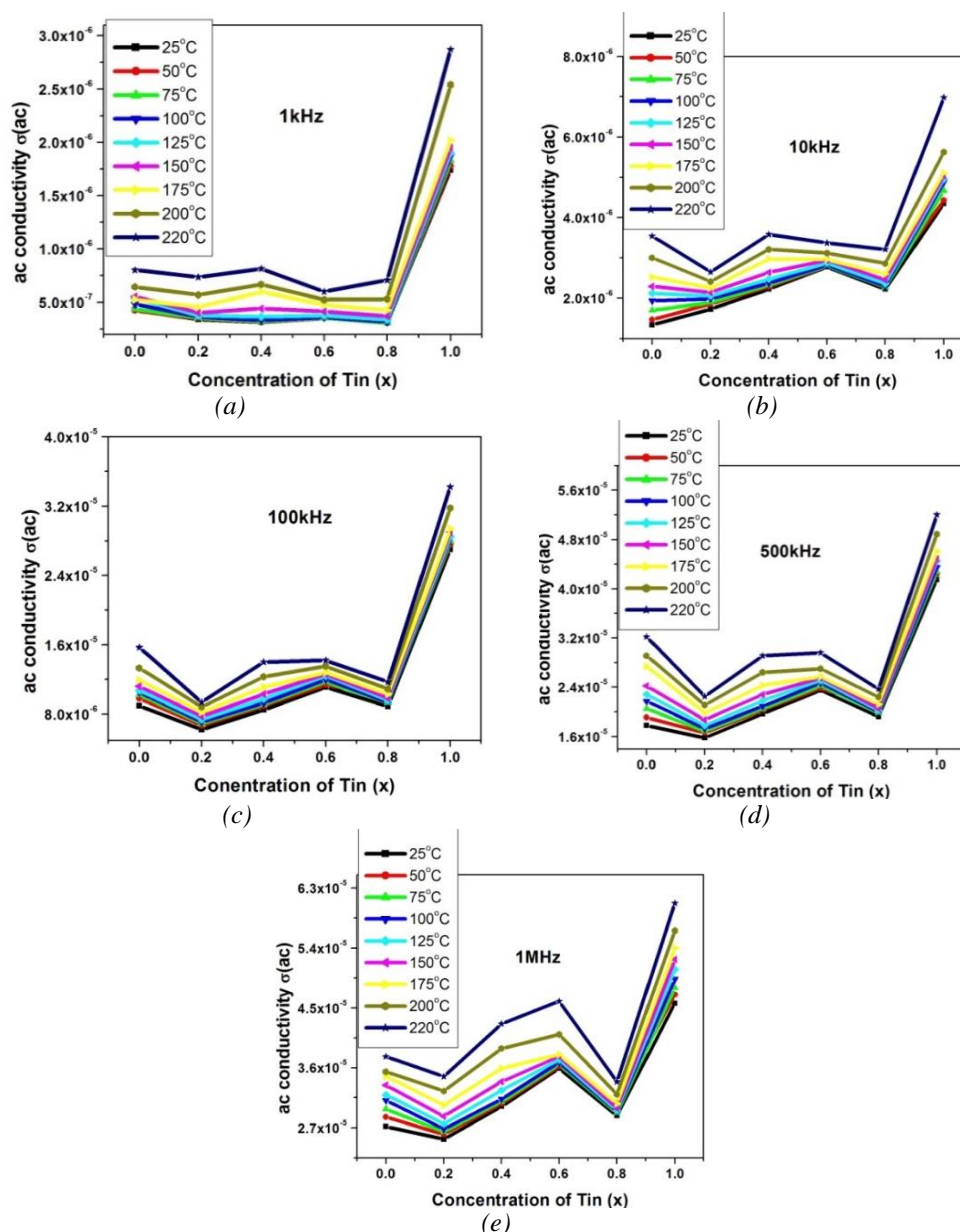


Fig. 9. AC conductivity (σ_{ac}) as a function of concentration of $\text{Sn}_x\text{Co}_{1-x}\text{Fe}_2\text{O}_4$ at frequency (a) 1kHz (b) 10kHz, (c) 100kHz, (d) 500kHz, (e) 1 MHz

Mechanism of dielectric properties

The ferrites consist of conducting particles that are isolated by insulating grain boundaries. When applied by an AC external field the mechanism of hopping occurs between $\text{Co}^{+2} \leftrightarrow \text{Co}^{+3}$ and $\text{Fe}^{+2} \leftrightarrow \text{Fe}^{+3}$. Hopping is a process in which electrons lose all its information after moving from one site to another. During the hopping process the electrons get access to the grain boundaries and charges add up as a result polarization is produced. This polarization is known as space charge polarization. Some time is taken by the charges in order to line-up to their axes along the AC applied field [28].

The dielectric constant, dielectric loss and ac conductivity increases with increase in the concentration due to their cation distribution. There are two sites in inverse spinel ferrites named as tetrahedral and octahedral sites. As cobalt ferrite is also has inverse spinel structure so Fe^{+2} ions are equivalently spread between A and B sites whereas Co^{+2} cations is only filled in B sites. The substitution of Sn^{+2} ions swaps the Fe^{+2} at tetrahedral site whereas Fe^{+2} ions migrate to octahedral sites replacing the Co^{+2} ions. As a result, Fe^{+2} ions decrease and Sn^{+2} increases at tetrahedral site

but on the octahedral site Co^{+2} decreases and Fe^{+2} ions increases which cause the increase in dielectric constant and dielectric tangent loss. Increase in the doping of tin enhances the conductivity due to fewer amounts of Co^{+2} ions at octahedral sites [29].

3.3.2 Variation of dielectric constant (ϵ') and dielectric loss (ϵ'') with frequency

The frequency response of the real part (ϵ') and imaginary part (ϵ'') of the dielectric constant of $\text{Sn}_x\text{Co}_{1-x}\text{Fe}_2\text{O}_4$ is shown in figure 10 and 11, with a frequency range from 1kHz, 10kHz, 100kHz, 500kHz, 1MHz. It is tailed from the graphs that dielectric constant (ϵ') and dielectric loss (ϵ'') show increasing trend at lower frequencies and decreases to minimum values with the increase in frequency. This is a normal trend in spinel ferrites [30].

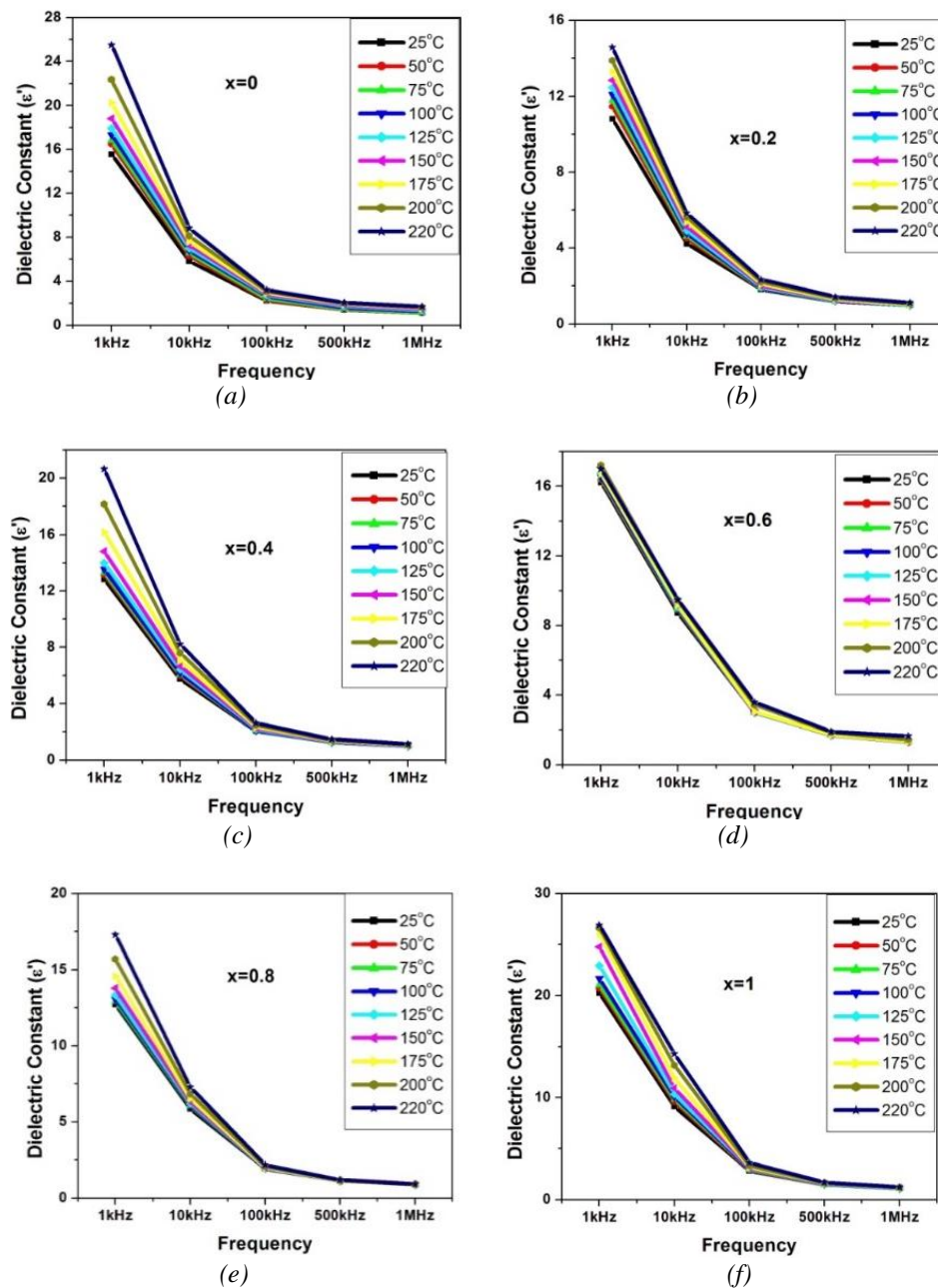


Fig. 10. Dielectric constant as a function of frequency at different temperatures at tin concentration (a) 0, (b) 0.2, (c) 0.4, (d) 0.6, (e) 0.8, (f) 1.0

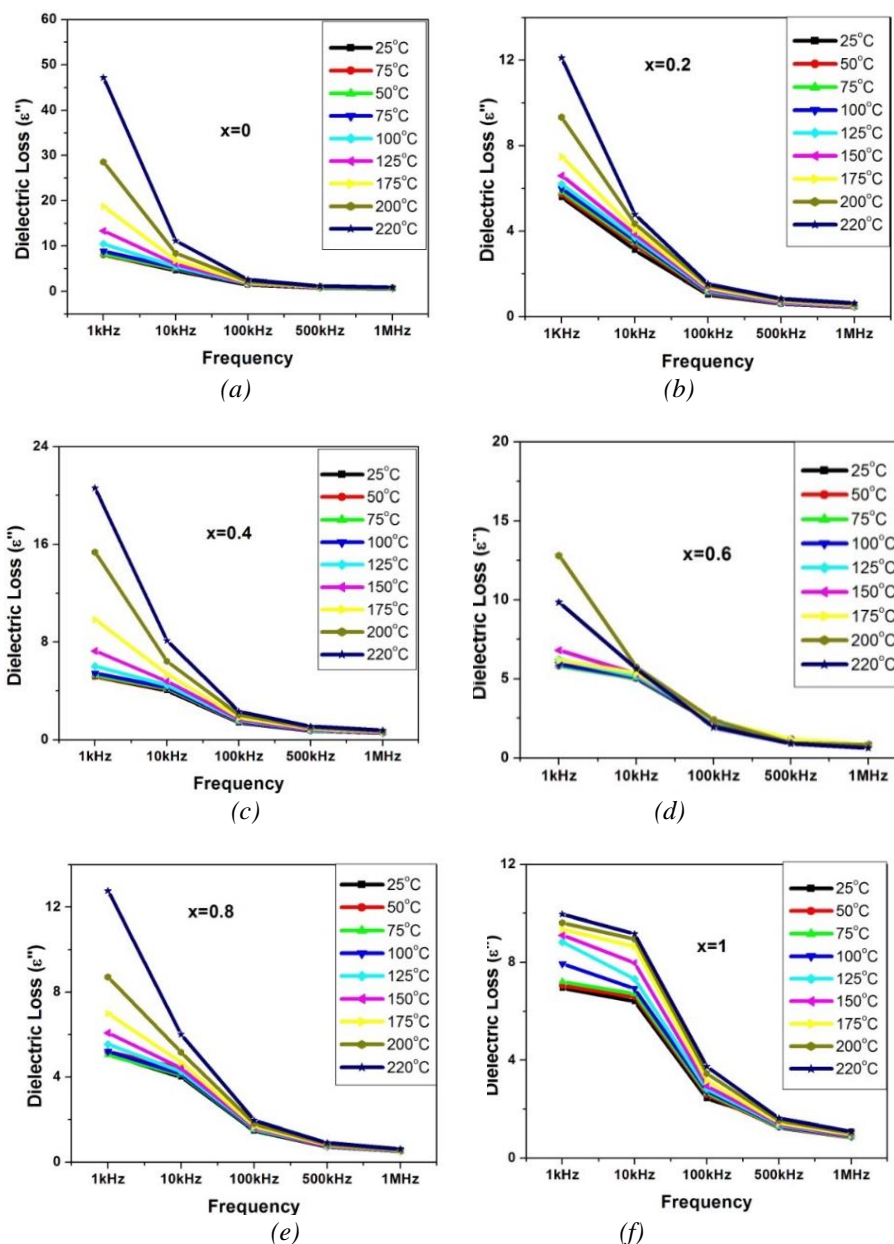


Fig. 11. Dielectric loss as a function of frequency at different temperatures at tin concentration (a) 0, (b) 0.2, (c) 0.4, (d) 0.6, (e) 0.8, (f) 1.0

The grain boundaries are extra vigorous at lower frequencies than grains in electrical conduction so the high values of dielectric constant (ϵ') and dielectric loss (ϵ'') are obtained. The dielectric constant (ϵ') curve represents the energy stored in the system as polarization whereas dielectric loss (ϵ'') shows the energy dissipated in the system [31]. The type of polarization observed by ferrites is known as interfacial polarization. The mechanism of polarization and conduction is same in ferrites. When an electron exchange occurs in Fe^{+2} ions i.e. $\text{Fe}^{+3} + e^{-1} \leftrightarrow \text{Fe}^{+2}$, these ions are unable to trail the external electric field. Due to this reason dielectric constant and dielectric loss has lower values at higher frequencies [32].

As tin occupies octahedral sites, these cations govern conductivity and polarization of the material, owing to their close vicinity. The Co^{+2} ions are substituted by Sn^{+2} or Sn^{+4} ions. The presence of double valance state of tin ions i.e. Sn^{+4} and Sn^{+2} are responsible for the electron exchange among these cations. Thus, the variation in the two valance states leads to an increase in the dielectric constant (ϵ') and dielectric loss (ϵ'') [33].

3.3.2.1 A.C conductivity response with respect to frequency

The ac conductivity (σ_{ac}) of $\text{Sn}_x\text{Co}_{1-x}\text{Fe}_2\text{O}_4$ as a function of frequency is shown in Fig. 12, with the frequency range from 1kHz, 10kHz, 100kHz, 500kHz and 1MHz. It is deduced using graphic illustrations that increasing the frequency the conductivity is increased. The frequency plays a vital role as pumping force for hopping of holes and electron in the material. Some of trapped charges in the material develop spontaneous behavior as a consequence of increase in the frequency which in turn leads to an increase in the conductivity of the doped sample. As mentioned earlier, tin ions occupy tetrahedral sites and the process of dielectric polarization and conduction is same in ferrites so hoping between Co^{+2} and Co^{+3} and electron hopping between Fe^{+2} - Fe^{+3} are accountable for conduction mechanism in cobalt ferrites [34]. Other than hole and electron hopping, variation in the tin ions valance states also causes an electron exchange i.e. $\text{Sn}^{+2} \leftrightarrow \text{Sn}^{+4} + 2e^{-}$ hence, contributes in the increase of conductivity of tin doped cobalt ferrites.

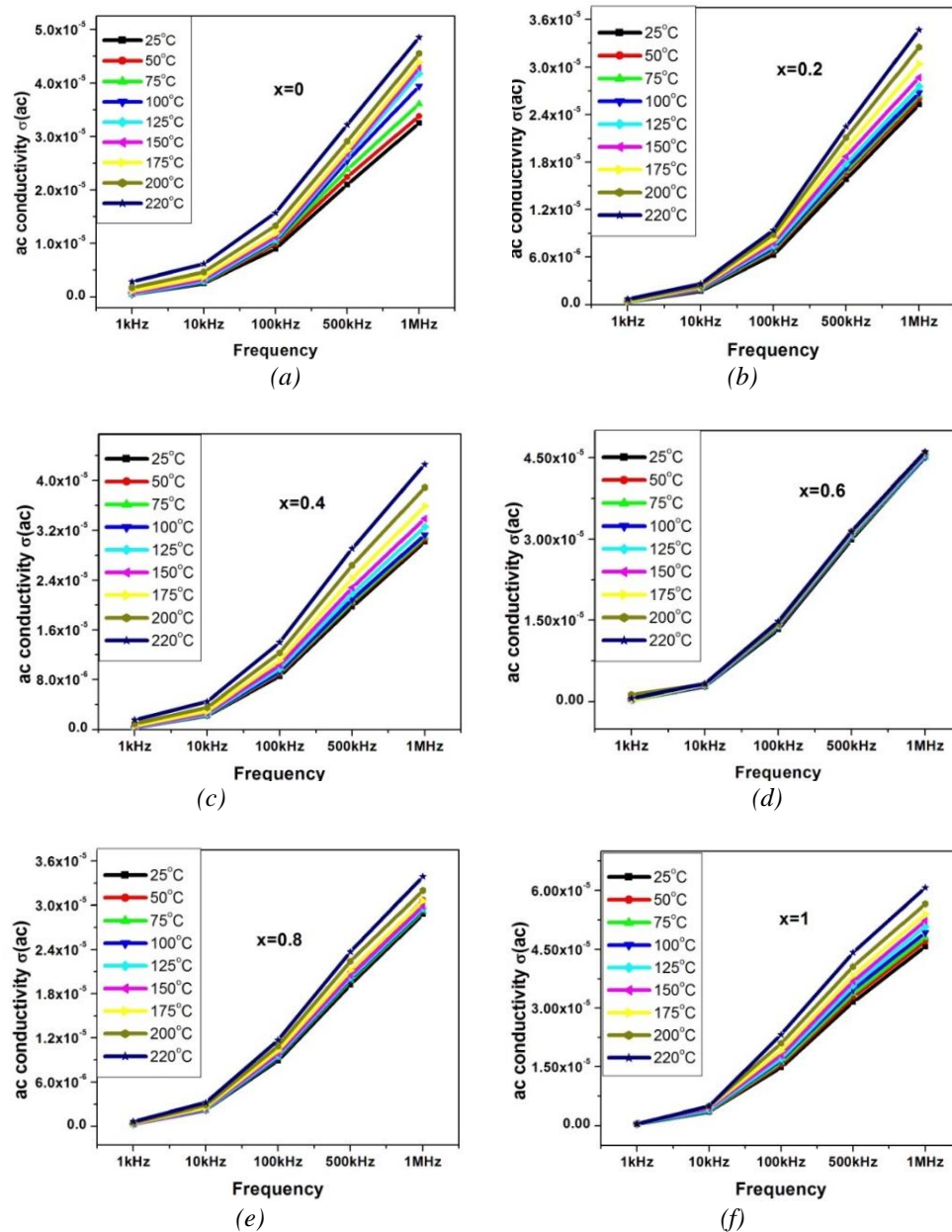


Fig. 12. A.C conductivity as a function if frequency at different temperatures at tin concentration (a) 0, (b) 0.2, (c) 0.4, (d) 0.6, (e) 0.8, (f) 1.0

3.3.2.2 Variation of dielectric constant, dielectric loss and ac conductivity as function of temperature

The fluctuation in the values of dielectric constant (ϵ'), dielectric loss (ϵ'') and ac conductivity (σ_{ac}) with temperature has been analyzed, with an extensive range of temperatures from 25°C to 200°C with an interval of 5°C at different frequencies. The frequency ranges are 1 kHz, 10 kHz, 100 kHz, 500 kHz and 1 MHz. The temperature dependency of the dielectric constant (ϵ') and dielectric loss (ϵ'') at particular frequencies is shown in Figs. 13, 14 and 15 respectively.

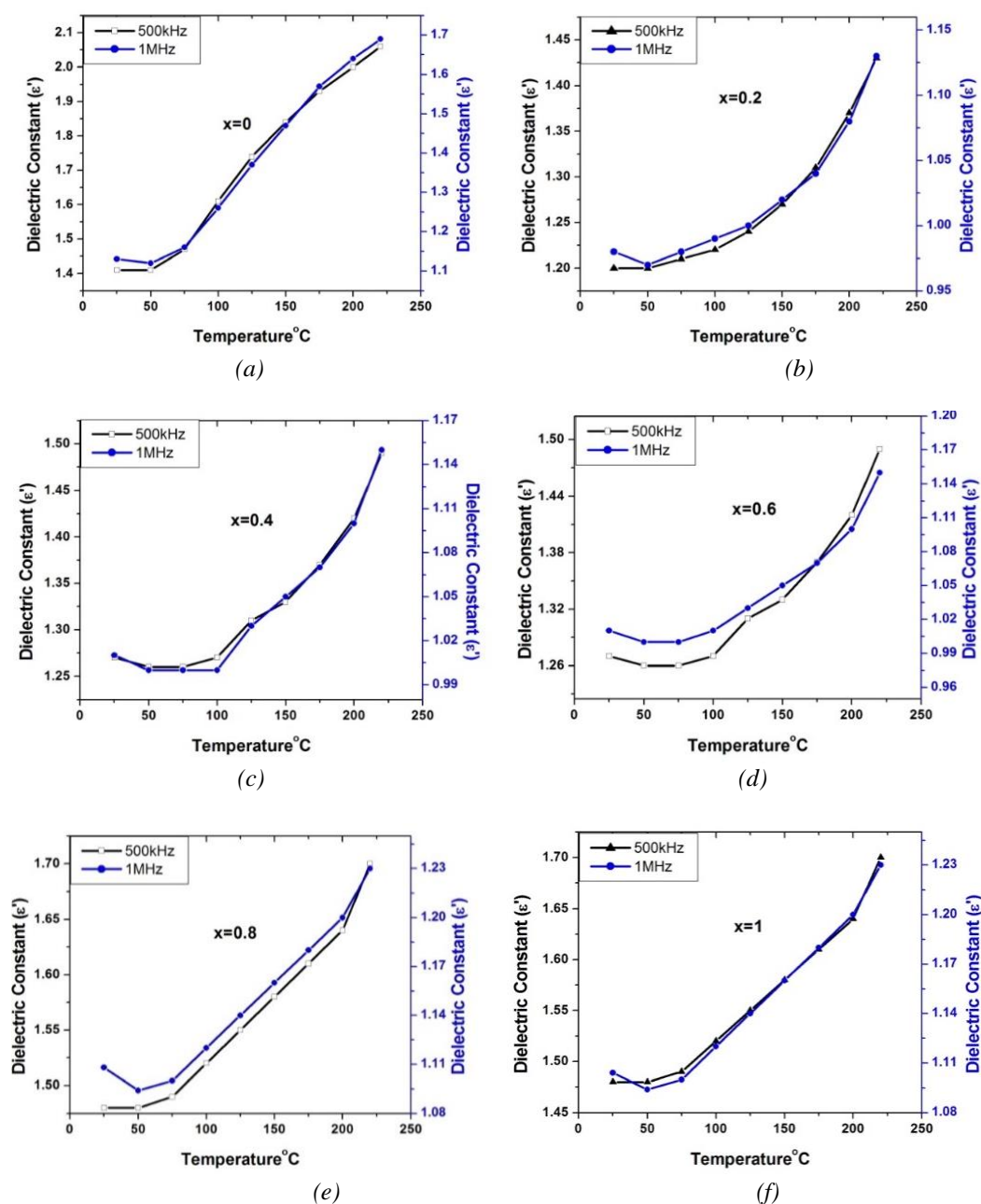


Fig. 13. Dielectric constant as a function of temperature of $\text{Sn}_x\text{Co}_{1-x}\text{Fe}_2\text{O}_4$ at (a) $x=0.0$, (b) $x=0.2$, (c) $x=0.4$, (d) $x=0.6$, (e) $x=0.8$, (f) $x=1.0$

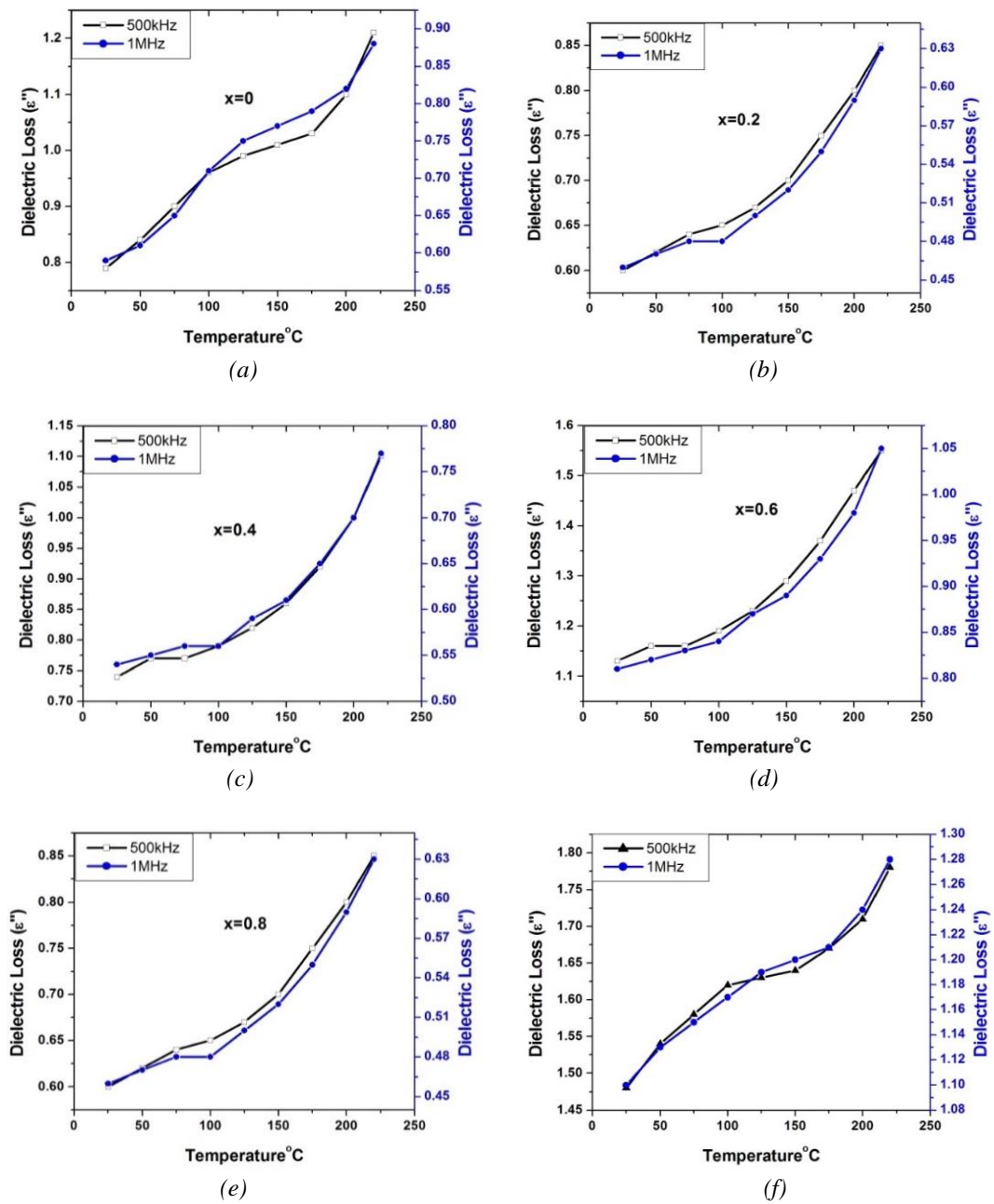


Fig. 14. Dielectric loss as a function of temperature at $\text{Sn}_x\text{Co}_{1-x}\text{Fe}_2\text{O}_4$ at (a) $x=0.0$, (b) $x=0.2$, (c) $x=0.4$, (d) $x=0.6$, (e) $x=0.8$, (f) $x=1.0$

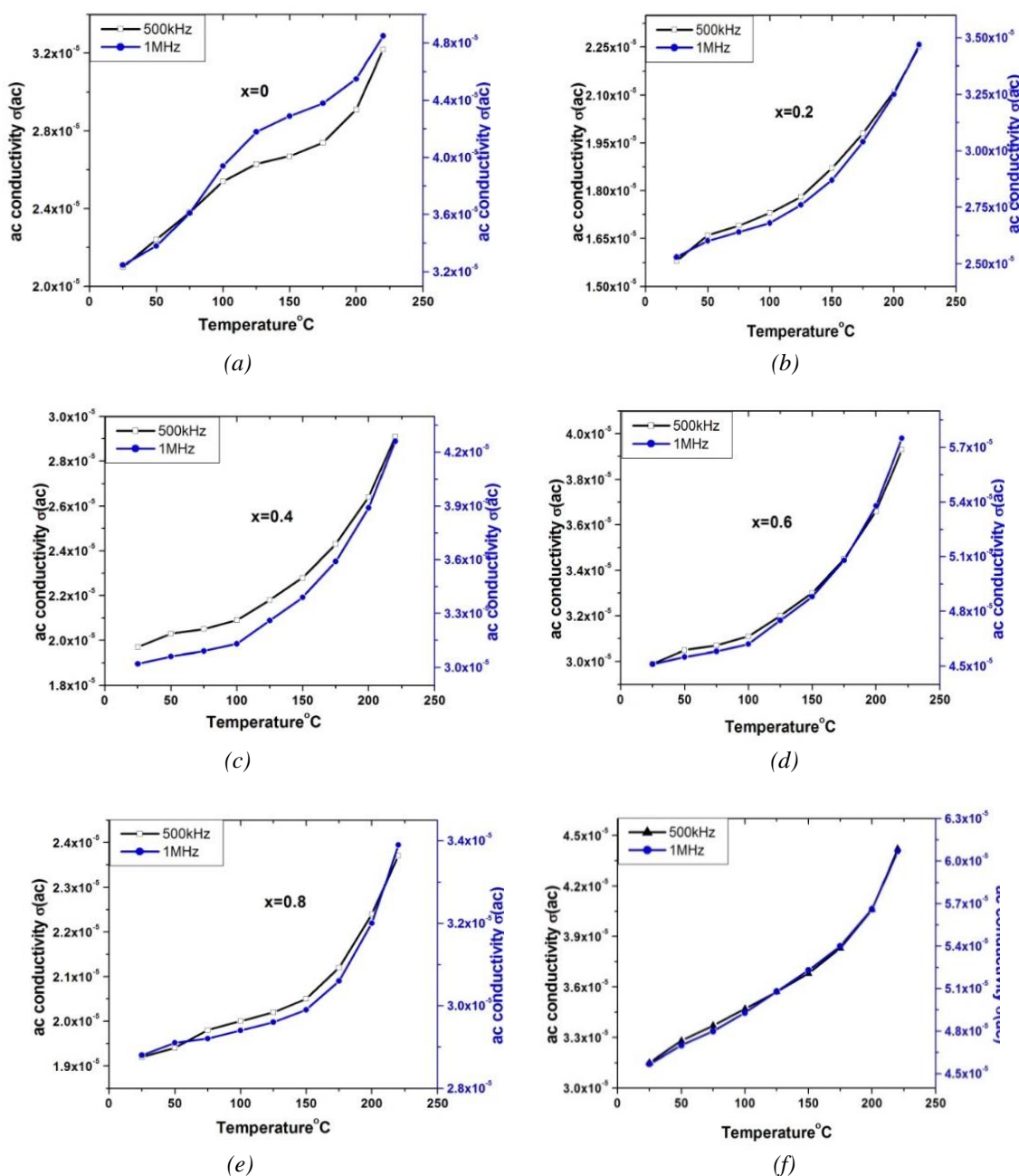


Fig. 15. AC conductivity as a function of temperature of $\text{Sn}_x\text{Co}_{1-x}\text{Fe}_2\text{O}_4$ at (a) $x=0.0$, (b) $x=0.2$, (c) $x=0.4$, (d) $x=0.6$, (e) $x=0.8$, (f) $x=1.0$

The influence of temperature on the conductivity of tin doped cobalt ferrites is shown in Fig. 15. The trend in the graph reveals that conductivity increases with increasing temperature. This response is observed because of the occurrence of a higher number of Fe^{+2} produced at higher temperatures. As a consequence of this phenomena, the probability of hopping between $\text{Fe}^{+2} \leftrightarrow \text{Fe}^{+3}$ increases, which in turn enhances the conductivity with an increase in the temperature. Another reason of increasing conductivity is correlated with decreasing porosity with the temperatures since pores are non-conductive and the charge carriers face the pores during hopping [35].

4. Conclusions

This research deals with preparation and characterization of tin substituted cobalt ferrites $\text{Sn}_x\text{Co}_{1-x}\text{Fe}_2\text{O}_4$ ($x=0, 0.2, 0.4, 0.6, 0.8, 1$) using simple ceramic route. It is discovered from the XRD results that inverse cubic spinel structure is formed.

The lattice parameter and crystallite size is found to increase with increasing tin content. LCR meter investigation reveals that increasing the tin concentration in cobalt ferrites decreases the tangent loss and improves the conductivity with the increasing frequency value; this excellent property of ferrites marks exceptional rank in applications of high frequency devices and microwave.

References

- [1] L. Zhao, H. Zhang, Y. Xing, S. Song, S. Yu, W. Shi, X. Guo, J. Yang, Y. Lei, F. Cao, J. Solid State Chem. **181**, 245 (2008).
- [2] M. George, S. S. Nair, K. A. Malini, P. A. Joy, M. R. Anantharaman, J. Phys. D **40**, 1593 (2007)
- [3] A. M. Shaikh, C. M. Kanamadi, B. K. Chougule, Mater. Chem. Phys. **93**, 548 (2005).
- [4] S. S. Shinde, K. M. Jadhav, Mater. Lett. **37**, 63 (1998).
- [5] A. M. M. Farea, S. Kumar, K. M. Batoo, A. Yousef, C. G. Lee, Alimuddin, J. Alloy Compd. **464**, 361 (2008)
- [6] C. C. Homes, T. Vogt, S. M. Shapiro, S. Wakimoto, A. P. Ramirez, Science **293**, 673 (2001).
- [7] Y.-C. Ma, J.-Z. Zhang, J. Zhao, Q.-S. Liu, Chin. Phys. Lett. **27**, 087701 (2010).
- [8] R. P. Mahajan, K. K. Patankar, M. B. Kothale, S. C. Chaudhari, V. L. Mathe, S. A. Patil, Pramana **58**(5-6), 1115 (2002).
- [9] G. H. Jonker, Journal of Physics and Chemistry of Solids **9**(2), 165 (1959).
- [10] J. G. Na, T. D. Lee, S. J. Park. " IEEE Transactions on Magnetics **28**(5), 2433 (1992).
- [11] J. G. Na, M. C. Kim, T. D. Lee, S. J. Park, IEEE Transactions on Magnetics **29**(6), 3520 (1993).
- [12] C. Fei, Y. Zhang, Z. Yang, Y. Liu, R. Xiong, J. Shi, X. Ruan, J. Magn. Magn. Mater. **323**, 1811 (2001).
- [13] S. Anjum, H. Nazli, F. Bashir, K. Mahmood, Materials Today: Proceedings **2**(10), 5552 (2015).
- [14] M. K. Shobana, Journal of Physics and Chemistry of Solids **73**(8), 1040 (2012).
- [15] S. Singhal, T. Namgyal, S. Bansal, K. Chandra, Journal of Electromagnetic Analysis and Applications 2010.
- [16] Mohamed, Mohamed Bakr, M. Yehia, Journal of Alloys and Compounds **615**, 181 (2014).
- [17] S. K. Gore, R. S. Mane, M. Naushad, S. S. Jadhav, M. K. Zate, Z. A. Allothman, B. K. N. Hui, Dalton Trans. **44**, 6384 (2015).
- [18] A. A. Yousif, M. E. Elzain, S. A. Mazen, H. H. Sutherland, M. H. Abdalla, S. F. Mansour, J. Phys. Condens. Matter **6**, 5717 (1994).
- [19] S. M. Attia, Egypt. J. Solids **29**, 2 (2006)
- [20] J. Smit, H. P. J. Wijn, Ferrites (Cleaver-Hume Press, London, 1959).
- [21] S. Singhal, T. Namgyal, S. Bansal, K. Chandra, Journal of Electromagnetic Analysis and Applications 2010 (2010).
- [22] A. Mukherjee, S. Basu, P. K. Manna, S. M. Yusuf, M. Pal J. Alloys. Comp. **598**, 142 (2014)
- [23] Safia Anjum, Hina Nazli, Farooq Bashir, Kiran Mehmood, Materials Today: Proceedings **2**(10), 5552 (2015).
- [24] K. Hannewald, V. M. Stojanovic, J. M. T. Schellekens, P. A. Bobbert, G. Kresse, J. Hafner, Phys. Rev. B **69**, 075211 (2004)
- [25] S. Anjum, S. Hameed, F. Bashir, Materials Today: Proceedings **2**(10), 5329 (2015).
- [26] N. H. Abdullah, A. N. Yusoff, J. Mater Sci **32**, 5817 (1997)

- [27] L. T. Robinkin, Z. I. N., Ferrites, IZV Acad. Nauk USSR, Minsk, 146,(1960).
- [28] C. G. Koops, Phys. Rev. **83**, 121 (1951).
- [29] S. Baijal, C. Prakash, P. Kishan, K. K. Laroia, J. Phys. C **17**,5993 (1984)
- [30] A. D. P. Rao, P. R. M. Rao, S. B. Raju, Materials Chemistry and Physics **65**, 90 (2000).
- [31] M. I. Kliger, Phys. Status Solidi B **79**, 1977.
- [32] N. Rezlescu, E. Rezlescu, Phys. Status Solidi A **23**, 575 (1974).